

Robust growth termination through local mechanical feedback in the *Drosophila* wing disc

Alexander Erlich*

LiPhy, CNRS–UMR 5588, Université Grenoble Alpes, F-38000 Grenoble, France

(Dated: November 3, 2020)

How does a cell in an organ know the overall size of the organ? It is thought that the *Drosophila* wing disc grows to the right size because its cells respond to both signalling proteins (morphogens) and mechanical stress. We show that size regulation can be achieved if cells respond exclusively to stress with an anisotropic growth response. To test this, we develop a continuum model which assumes the spatial uniformity of cell proliferation in the wing disc and predicts compression in the disc center, tension in its periphery, and a sigmoidal evolution of the disc size, all of which have been observed in experiments. We further show that the addition of a basal growth term is necessary for the wing disc to always reach the same size. Contrary to the current paradigm, our results suggest that local mechanical feedback is the primary mechanism in regulating the final disc size.

I. INTRODUCTION

How does a cell in an organ know what overall size the organ has? How does the cell decide when to stop dividing once the organ has reached the right size? The mechanisms with which cells measure the dimension of the organ to regulate their growth remains a classical mystery in developmental biology [3].

The *Drosophila* wing forms from a sac of undifferentiated epithelial cells termed the wing imaginal disc (Fig. 1A), which grows within the first 100 hours of development approximately by a factor of 1000, reaching its final size [4, 5]. The size regulation of the wing disc is extremely robust: the wing reaches normal size even if its development time is shortened, or if a portion of the cells is killed [6]. Signalling proteins called morphogens have been found to restrict and promote growth [7], and have received most attention as a tool to explain size regulation. However, morphogenetic growth models alone fail to explain numerous experimental observations in the wing disc [8].

It has become widely accepted that in addition to biochemical signals, mechanical cues have an impact on growth regulation [9, 10]. Indeed, in many tissue stretching stimulates cell proliferation, whereas compression inhibits it [9, 11, 12]. This causes a buildup of mechanical stress, as the regions that have locally expanded more than their surroundings push on their neighbors. Through this mechanism known as "*differential growth*", many living tissues are known to actively build and maintain internal mechanical stresses [13–19]. The presence of stresses can be observed with a naked eye, when the integrity of the tissue is broken: arteries open when radially cut, and Wapas (known as "killer trees" in French Guiana) explode when logged, due to the sudden release of internal stresses.

In light of the emerging link between mechanics and growth control in the *Drosophila* wing disc, which is be-

ing developed through models [20–22] and at the signalling level [23], we explore the hypothesis that size control is achieved in the wing disc exclusively, or primarily, through local mechanical feedback. This is in contrast to the currently held view in which mechanics plays at most a supporting role for morphogens in size regulation [21, 22]. Our goal is to gain a fundamental understanding of the role of mechanics in size control of the wing disc, and its relative importance in size regulation compared to other factors such as morphogens.

A key experimental observation is that the cell proliferation in the wing disc is spatially uniform for all developmental times [12, 24, 25]. However, both the principal morphogen field [4, 26] and the stress field are spatially non-uniform in the wing disc (see Fig. 1). It remains a challenge for modelling to explain the uniformity of cell proliferation in the entire domain via local feedback from non-uniform fields like morphogens and stress. Shraiman [20] proposed a feedback mechanism between growth and mechanics that explains the spatial uniformity of growth. However, his model lacks growth termination, growth is therefore unbounded. It is only through the combination of mechanical feedback and a morphogen field that growth termination has previously been explained [21, 22]. In these models the role of mechanics is to average any heterogeneity in growth by local mechanical feedback, any transient overgrowth is suppressed through mechanical feedback. However, some of the models may need to be revisited in light of newer experimental discoveries: The non-scaling morphogen modeled in [21] has been experimentally corrected [4]. Additionally, the initially transient phase of non-uniform growth modeled in [21, 22] has not been experimentally substantiated [4, 12, 25, 27].

It is known that stress can be built through growth broadly in two ways: Non-uniformity and anisotropy [28]. Anisotropy has been overlooked by previous size control models which focused on non-uniformity [20–22]. Our focus in this study is on size control through anisotropic growth. The idea is illustrated in Fig. 2. The local increase in mass, modeled through the growth tensor G , causes the tissue to grow at different rates in different

* alexander.erlich@univ-grenoble-alpes.fr

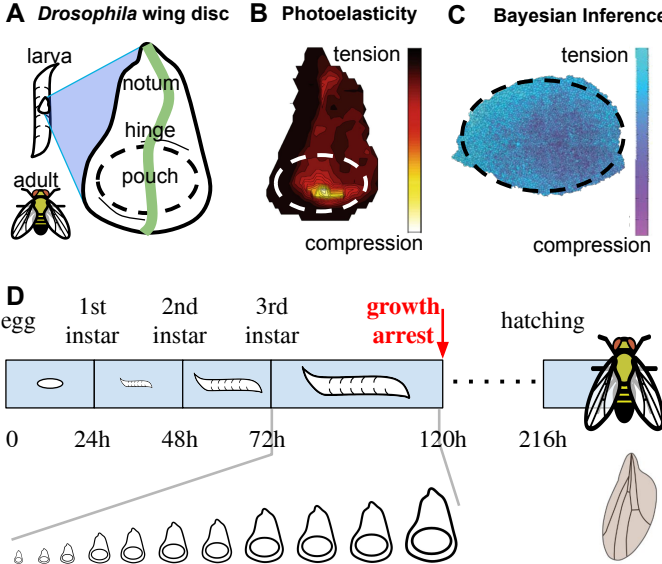


FIG. 1. Mechanics and growth arrest of the *Drosophila* wing disc. (A) Sketch of *Drosophila* wing disc. The center of the pouch (dashed region) is in compression, the rest of the wing disc (which comprises pouch, hinge and notum) is in tension. (B) Photo-elasticity measurements showing optical retardance [1]. The retardance is highest in the centre of the imaginal wing disc, showing that this region is subjected to the highest compression. (C) Distribution of hydrostatic pressure differences in a wing disc, as inferred from the cell geometries [2], showing once again compression at the pouch center and tension at the periphery. (D) In approximately four days, the wing disc undergoes rapid growth, after which cell proliferation gradually slows down and comes to a halt, at around 120 hours after egg laying. At this point the wing size is fixed. In subsequent morphological stages (pupation and hatching) the wing size stays the same.

directions (here: radial vs tangential direction) in a spatially uniform way. In this article, we propose a theoretical framework for the interplay between local mechanical stresses and growth control, which we refer to as a mechanical feedback mechanism. A key feature of our model is that the growth response is anisotropic, allowing us to preserve growth uniformity in line with recent experimental evidence. Our approach is consistent with other experimental observations, such as increased tension in the disc periphery, and a sigmoidal evolution of size which leads to growth termination. To guarantee that a pre-encoded disc size is reached robustly during development, we amend the local mechanical feedback mechanism with a basal growth. Unlike previous mechanics-based models which relied on computation [5, 21, 22], our continuum model allows us to give explicit expressions for the final size of the tissue and the parameters it is regulated by. This approach provides a mechanism for the homogeneous growth and buildup of compressive stresses at the center and tensile stresses at the periphery observed during the growth of the wing disk of the developing fly.

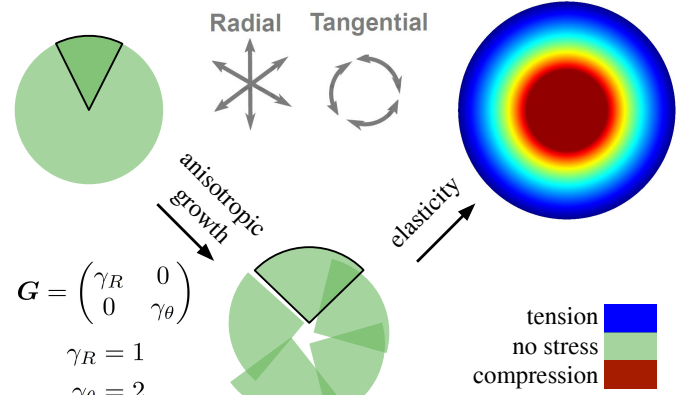


FIG. 2. How stress is built through anisotropic growth. The top left drawing shows a sketch of the unstressed wing disc before any growth has occurred, highlighting a pizza-shaped segment. Growth, i.e. the local addition of mass, is modeled through the growth tensor \mathbf{G} . For purely anisotropic growth, the growth γ_R in radial direction is different from that in tangential direction γ_θ . In this illustration we assume no growth in radial direction $\gamma_R = 1$ and some growth in tangential direction $\gamma_\theta > 1$. Such an addition of mass would increase the angle of every segment, causing pieces to overlap and no longer fit into a disk geometry (middle drawing). The pieces can be fit together into a disk through elasticity, i.e. local tension and compression, which results in a bigger overall size of the disk due to growth (top right drawing). This modelling approach is known as deformation gradient decomposition [16, 28].

II. RESULTS

A. Local mechanical feedback and homeostasis

To understand how stress is used to robustly achieve growth termination and size regulation in the imaginal disc, we propose a continuum model of growth dynamics based on the framework of morpho-elasticity [28, 29]. A continuum mechanical framework is natural because the growth rate is uniform and stress is a macroscopic quantity. The centerpiece of the model is the "growth law" which describes the local feedback mechanism between growth and mechanics:

$$\dot{\mathbf{G}}\mathbf{G}^{-1} = \mathbf{K}(\mathbf{T}_{\text{dev}} - \mathbf{T}^*). \quad (1)$$

The growth rate $\dot{\mathbf{G}}\mathbf{G}^{-1}$ represents the relative volume increase over time at all points in the tissue. The growth rate is proportional to the difference of the deviatoric (traceless) part of the Cauchy stress tensor \mathbf{T}_{dev} and the homeostatic stress \mathbf{T}^* . The constant coefficient matrix \mathbf{K} dictates how fast the system reaches homeostasis. The unit of \mathbf{K} is an inverse viscosity. A novelty compared to existing models of the type (1) [30–36] is that the mechanical feedback mechanism depends on the deviatoric part of Cauchy stress \mathbf{T}_{dev} rather than the Cauchy stress \mathbf{T} itself. As will be explained in Section II B, this choice

is a result of encoding spatially uniform growth into the model (i.e. all components of \mathbf{G} are spatially constant) as suggested by experimental observations in the *Drosophila* wing disc [4, 12, 27].

The model relies on the idea of mechanical homeostasis [29, 36, 37], which is that each cell has an encoded preferred state of mechanical stress (the homeostatic stress). When the cell is locally stretched compared to its homeostasis cell proliferation is stimulated, whereas if the cell is compressed compared to its homeostasis growth is inhibited. Mechanical homeostasis is consistent with the experimental observation that stretching stimulates cell proliferation, whereas compression inhibits it [9, 11, 12]. Mechanical homeostasis is realised in the model through a linear coupling of the growth deformation tensor \mathbf{G} to the difference between the deviatoric stress tensor \mathbf{T}_{dev} and the homeostatic stress \mathbf{T}^* . When the deviatoric stress tensor has reached the prescribed value of homeostatic stress ($\mathbf{T}_{\text{dev}} = \mathbf{T}^*$), growth stops ($\dot{\mathbf{G}} = 0$). The growth law (1) is supported by thermodynamic arguments taking into account tissue dissipation [33, 38]. It is solved in conjunction with mechanical stress balance and a non-linear elastic stress-strain relationship which supports large tissue deformations, see further details in the Supplementary Information.

B. Dynamics of growth and final size of wing disc

To explain how the mechanical feedback mechanism (1) ensures spatially uniform growth, we model the *Drosophila* wing disc as an incompressible isotropic hyperelastic material. We express all tensor quantities in the polar coordinate basis, where they take diagonal form: growth tensor $\mathbf{G} = \text{diag}(\gamma_R, \gamma_\theta)$, Cauchy stress $\mathbf{T} = \text{diag}(T_R, T_\theta)$, growth coefficients $\mathbf{K} = \text{diag}(K_R, K_\theta)$, where the subscript R denotes the radial direction and θ denotes the tangential direction (see insets in Fig. 3A for illustration of radial and tangential directions). For instance, the growth tensor $\mathbf{G} = \text{diag}(\gamma_R, \gamma_\theta)$ has the components γ_R, γ_θ , representing the local addition of material in radial and tangential direction, respectively. We further assume that \mathbf{G} is spatially uniform, that is $\partial\gamma_R/\partial R = \partial\gamma_\theta/\partial R = 0$. The Cauchy stress can be written as the sum of deviatoric and hydrostatic stresses, $\mathbf{T} = \mathbf{T}_{\text{dev}} + \mathbf{T}_{\text{hyd}}$. The two contributions to the Cauchy stress tensor (which are derived in detail in the Supplementary Information) are:

$$\mathbf{T}_{\text{dev}} = \begin{pmatrix} T_{\max} & 0 \\ 0 & -T_{\max} \end{pmatrix}, \quad \mathbf{T}_{\text{hyd}} = \begin{pmatrix} -P & 0 \\ 0 & -P \end{pmatrix}, \quad (2)$$

where the hydrostatic pressure is

$$P = T_{\max} \left[1 + 2 \log \left(\frac{R}{R_{\text{initial}}} \right) \right]. \quad (3)$$

Here the relative position in radial direction R/R_{initial} ranges from 0 to 1. The maximal shear stress T_{\max} is

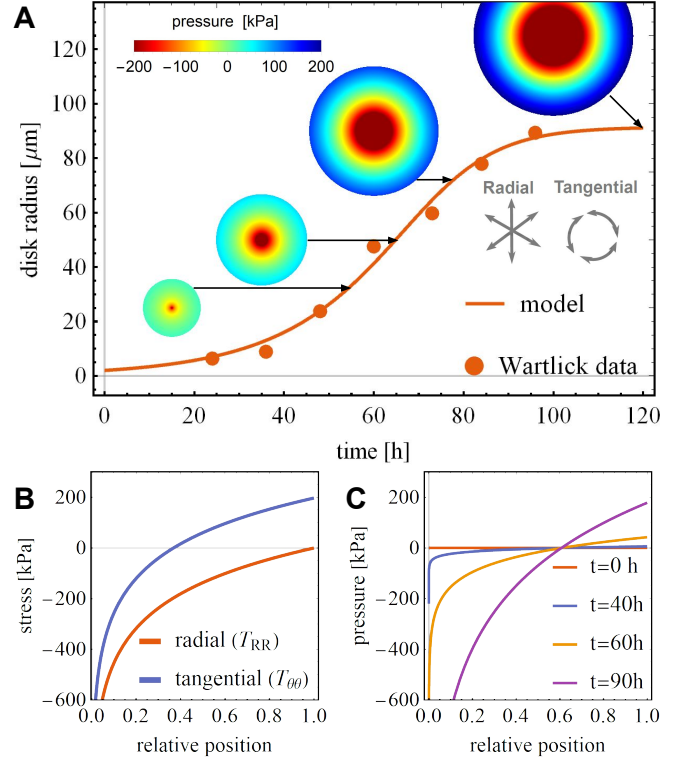


FIG. 3. A model of growth dynamics driven by mechanical stress. **A** Growth termination occurs in sigmoidal fashion, in line with experimental measurements in *Drosophila* wing disc. A good fit to the data of Wartlick [4] is obtained. The insets show the disc size and distribution of pressure for the developmental times $t = 55$ h, $t = 66$ h, $t = 79$ h and $t = 120$ h after egg laying. Model parameters can be found in Table II, fit parameters in Table I. **B** Typical stress profiles during growth dynamics. The radial stress is always compressive. The hoop stress is compressive near the disc center and tensile at the periphery. **C** Pressure, its evolution, vanishes for large times towards growth termination.

given by

$$T_{\max} = \frac{\mu}{2} \left(\frac{\gamma_\theta}{\gamma_R} - \frac{\gamma_R}{\gamma_\theta} \right), \quad (4)$$

where μ is the shear modulus of the tissue. We notice that the deviatoric part \mathbf{T}_{dev} according to (2)₁ and (4) is spatially uniform, but the hydrostatic part \mathbf{T}_{hyd} according to (2)₂ and (3) is not. This observation makes deviatoric stress the natural choice for the growth law (1), as it preserves the uniformity of \mathbf{G} and therefore the proliferation rate. We choose the growth rates $\mathbf{K} = \text{diag}(K_R, -K_\theta)$, as well as an isotropic homeostatic stress, $\mathbf{T}^* = \text{diag}(\mathbf{T}^*, \mathbf{T}^*)$. In this case the growth dynamics (1) is driven by maximal shear stress (similarly to [39]) and homeostatic stress (similarly to [37]):

$$\dot{\gamma}_R \gamma_R^{-1} = K_R (T_{\max} - T^*) \quad (5)$$

$$\dot{\gamma}_\theta \gamma_\theta^{-1} = K_\theta (T_{\max} - T^*) \quad (6)$$

Note that the model (5), (6) requires that cells can orient themselves in the tissue, distinguishing the principal directions (radial and tangential). We hypothesise that such orientation is possible because peripheral cells become increasingly elongated [40], and epithelial cell shape, principal directions of stress, and cell division are closely related [41, 42]. For the sake of analytical transparency, we first consider a simplified subcase in which mechanical feedback only works in radial direction and there is no growth in tangential direction ($K_\theta = 0$, $\gamma_\theta = 1$), the system simplifies to a single non-linear ordinary differential equation

$$\dot{\gamma}_R \gamma_R^{-1} = K_R \left(\frac{\mu}{\gamma_R} - \mu \gamma_R - T^* \right), \quad \gamma_R(0) = 1. \quad (7)$$

Here, we assumed that at $t = 0$ the system starts in an ungrown, unstressed state, that is $\gamma_R = 1$. The system (7) can be fully solved analytically (the full expression is given in the Supplementary Information). The disc size follows a sigmoidal form as seen in Fig. 3. A good fit to the data of Wartlick [4] is obtained (Fig. 3), using two fit parameters, the time scale $(\mu K_R)^{-1}$ and the non-dimensional homeostatic stress T^*/μ (the fit parameters are documented in Table I, column "only radial MF"). The model is consistent with the experimental observation that growth rates are uniform [12, 24, 25], that stresses are compressive at the disc center and tensile at the periphery [1, 2], and that as the wing disc grows cells in the center of the developing wing become more compressed [43].

The model (7) is consistent with the experimental observations of the increased buildup of stress in the wing disc. Experimental data of 2d slices of wing pouch tissue show that cells at the periphery become increasingly elongated [40]. Given that cells in the wing pouch are also volume preserving [43], tangentially elongated cells at the periphery imply a tensile stress in tangential direction, as concluded in [39]. This trend is visible from area measurements of cells in the developing wing disc, see Fig. 4A. Over the course of development, cells in 2d slices at the periphery of pouch have larger areas, and are increasingly elongated, suggesting an increase in peripheral tension in tangential direction. This trend is qualitatively consistent with the stress measurements and increase in disc size, see Fig. 4B. We expect this qualitative trend between model and experiment to become quantifiable once image-based force reconstruction algorithms such as [2] are applied to the same wing disc at different developmental times.

As the size of the wing disc follows a sigmoidal form shown in Fig. 3A, it converges to an asymptotic size corresponding to the final size at growth termination. The model (7) predicts the final radius given by

$$R_{\text{final}} = R_{\text{initial}} \sqrt{\frac{\sqrt{(T^*)^2 + 4\mu^2} - T^*}{2\mu}}. \quad (8)$$

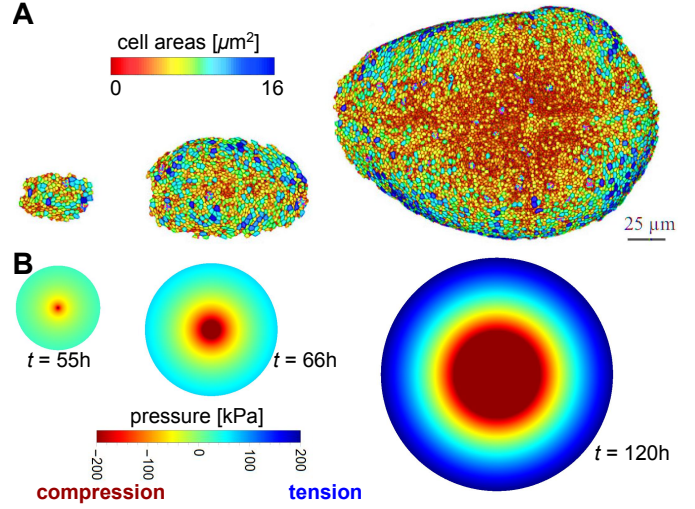


FIG. 4. Trends in the developing wing disc. **A** Live imaging measurements of wing pouch cell areas at different experimental times, adapted from [5]. Cell areas become gradually larger in the pouch periphery, while the overall cell volumes remain constant [43], suggesting that there is a buildup of mechanical stress at the periphery. **B** Model results qualitatively match the experimental observation, showing a similar trend in disc size as well as a buildup of pressure at the disc periphery.

The disc reaches a point of fastest growth, corresponding to the inflection point of the sigmoid (around $t = 60$ h in Fig. 3A). The model (7) allows us to calculate the development time at which the inflection point is reached:

$$t_{\text{inflection}} = \frac{1}{K_R} f(T^*, \mu). \quad (9)$$

The full form of f is given in the Supplementary Information. We can extract from the explicit expressions (8) and (9) how the parameters control the transient dynamics and the final size of the wing disc. The homeostatic stress value T^* sets the asymptote, i.e. final radius, of the wing disc: The larger the absolute value of the homeostatic stress $|T^*|$ is, the larger is the final radius, see Fig. 5A. The growth rate K_R , on the other hand, sets the inflection point of the sigmoid curve: For larger growth rates the inflection point moves to an earlier development time, the wing disc gets to its final size faster (Fig. 5B).

C. Robustness of growth termination

While our model exhibits growth termination, it is important to investigate if this termination robustly reproduces a pre-encoded final size, irrespective of small perturbations in initial growth rates (at time $t = 0$ of the simulation). To this end, we solve the system (5) and (6) with varying initial growth rates γ_R and γ_θ at $t = 0$, corresponding to an initial radius $R_{\text{initial}} \sim \sqrt{\gamma_R \gamma_\theta}$ at $t = 0$. The evolution of the wing disc size is shown in

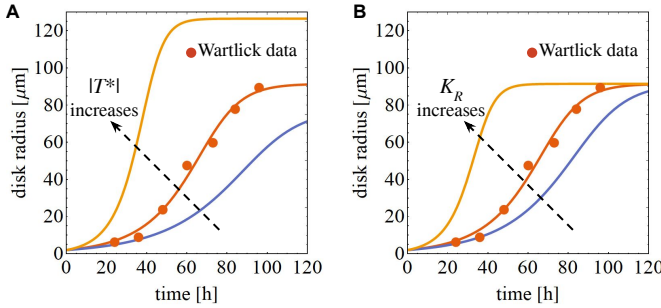


FIG. 5. The homeostatic stress changes the final disc size, whereas the growth rate changes the inflection point of the growth curve. **A** The larger the absolute value of the homeostatic stress is T^* , the larger is the final disc size. Parameter values are $T^* = -1.5 \text{ MPa}$ for the blue curve, $T^* = -2.1 \text{ MPa}$ for the red curve and $T^* = -4.0 \text{ MPa}$ for the orange curve. **B** The larger the growth rate K_R , the earlier the inflection point of the sigmoid. Parameter values are $4.00 \cdot 10^{-6} \text{ kPa}^{-1} \cdot \text{hours}^{-1}$ for the blue curve, $5.01 \cdot 10^{-6} \text{ kPa}^{-1} \cdot \text{hours}^{-1}$ for the red curve and $10.00 \cdot 10^{-6} \text{ kPa}^{-1} \cdot \text{hours}^{-1}$ for the orange curve. For all simulations, $\mu = 10 \text{ kPa}$, $R_{\text{initial}} = 2 \mu\text{m}$.

Fig. 6A alongside a fit of the Wartlick [4] data (in red). The blue and yellow curves in Fig. 6A are based on the same parameters but slightly altered initial growth rates. We show that small changes in conditions in the initial growth rates produce vastly different final sizes. The same three curves are shown in Fig. 6B in the phase space of growth, plotting tangential over radial growth. The dashed line corresponds to growth termination. All curves eventually terminate on the dashed line, however each point on that dashed line corresponds to a different final radius. The reason for the non-robustness of this model to encoding a pre-defined size is that the stress in the wing disc geometry does not scale with an isotropic growth of the wing disc, consistent with [44]: Rescaling the growth tensor by some factor α leads the size of the body to be α times as large, but the stress components do not change under such a transformation.

We propose a modification of (1) which allows to robustly encode the final size of the wing disc. The model relies (as before) on local mechanical feedback, added to a local feedback of proliferation rate:

$$\dot{\mathbf{G}}\mathbf{G}^{-1} = \mathbf{K}(\mathbf{T}_{\text{dev}} - \mathbf{T}^*) - s\mathbf{G} \quad (10)$$

Here s is a scalar constant in space and time. To interpret the term $s\mathbf{G}$, we consider the the absence of mechanical feedback $\mathbf{K} = 0$. In the relevant parameter regime in which s is much smaller than the time scale of growth termination (see Table I), the term $s\mathbf{G}$ would act like a basal growth rate [45, 46]. In the latter case, the growth rate $\dot{\gamma}\gamma^{-1} = -s$ adds the same pre-encoded amount of biomass per unit of time regardless of external conditions. We therefore term the contribution $s\mathbf{G}$ "basal growth". We consider the growth dynamics of (10) in Fig. 6C and D. We can see that changes in the initial geometry lead to the same asymptotic final size (Fig. 6C). This corre-

sponds to a single stable equilibrium point in the phase space of growth (Fig. 6C) which all trajectories despite some perturbations in initial growth rates converge to. The final size of the wing disc is robustly encoded in this equilibrium point. It is given by

$$R_{\text{final}} = R_{\text{initial}} \sqrt{\frac{(\mu K_R^2 - \mu K_\theta^2 + K_R K_\theta T^*)^2}{K_R K_\theta s^2}}. \quad (11)$$

The final size depends on the the shear modulus μ , the radial and tangential growth responses K_R , K_θ , and the rate of basal growth s .

We can summarise (10) into three distinct scenarios:

- 1. Only basal growth, no growth termination** ($s \neq 0$, $\mathbf{K} = 0$): The proliferation rate is a function of growth itself. Depending on the sign of s , the tissue will either grow or shrink without a bound. There is no mechanism to slow down growth/shrinking.
- 2. Only mechanical feedback, non-robust growth termination** ($s = 0$, $\mathbf{K} \neq 0$): Local mechanical feedback alone produces growth termination, in which the size of the wing disc follows a sigmoidal profile. However, the final size of the disc is sensitive to growth rates at the initial growth rates (at time $t = 0$ in the simulation). The model does not robustly encode a final disc size, see Fig. 6A and B.
- 3. Mechanical feedback with basal growth, robust growth termination** ($s \neq 0$, $\mathbf{K} \neq 0$): Robust encoding of the final size of the wing disc irrespective initial growth rates, see 6C and D.

III. DISCUSSION

We discuss a long standing question in the study of growth and size regulation of *Drosophila*: Through which mechanism can the final size of the wing disc be robustly encoded, and how can such a law maintain uniform proliferation rates along the disc despite the fact that its input field (mechanical stress) is becomes increasingly heterogeneous?

We show that growth termination can be explained through local mechanical feedback alone. This expands previous work according to which mechanical feedback can explain the uniformity of growth [20], but not growth termination. Indeed, the current viewpoint in literature is that growth termination results from morphogens alone [26, 50], or a combination of morphogens and local mechanical feedback, [21, 22]. In the latter scenario, mechanics takes a secondary role, smoothening out transient uniformity of growth. We provide an alternative perspective in which mechanics takes the primary role in growth termination, wheres morphogens could take an

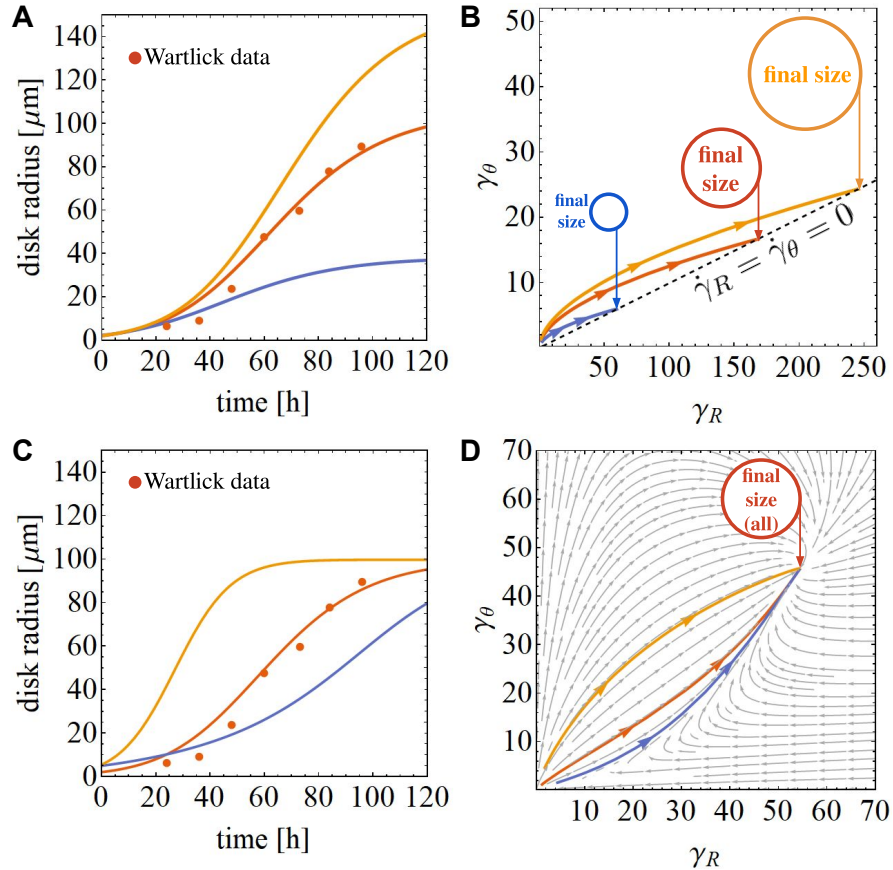


FIG. 6. Robustness of size control. **A** In the mechanical feedback model (1), a small change in the initial condition drastically changes the final disc size. The model thus captures growth termination (i.e. growth rates slow down and the system reaches a final size) but not size regulation (i.e. the encoding of a precise final size). The initial conditions are $(\gamma_R, \gamma_\theta)$ at $t = 0$ are $(1, 1)$ for the red curve, $(1.54, 0.8)$ for the blue curve and $(0.93, 1.14)$ for the orange curve. **B** The same data shown in the phase space of growth. All curves reach growth termination (dashed line) but they terminate at different final sizes (insets). This implies that size is not encoded robustly in a feedback mechanism between growth and mechanics alone. **C** The addition of basal growth to mechanical feedback, according to the model (10), is no longer sensitive to initial conditions. The same final size, encoded by the parameters shown in (11), is always attained. This model captures size regulation. The initial conditions are $(\gamma_R, \gamma_\theta)$ are $(1, 1)$ for the red curve, $(6.2, 2.2)$ for the blue curve and $(2.5, 6.6)$ for the orange curve. **D** All curves terminate at the same final size.

auxiliary role in making the encoding of a specific size more robust, by endowing the system with a morphogen diffusional length scale.

We further expand the important question of robustness of morphogenesis [51]. Our model combines local mechanical feedback and the local cell growth to robustly encode a final disc size that is reached even if the initial growth rates (at $t = 0$ in the simulation) are perturbed. This is consistent with experimental results according to which the final size of the wing disc is highly robust with respect to mechanical and chemical perturbations [6].

We find that a coupling of growth rate to deviatoric stress, rather than the traditionally used Cauchy stress [28, 31, 33], allows for the experimentally observed spatial uniformity of the growth rate. We present a model for local mechanical feedback in which growth is driven by deviatoric stress (as recently proposed in the context of

the wing disc [39]) and a homeostatic stress. This mechanism is the first to account for the uniformity of growth while at the same time allowing a buildup of stress during morphogenesis, as well as growth termination.

A major next step in the modelling of *Drosophila*, and potentially its size regulation, is to understand the 3d structure of the wing disc. The wing disc forms a sac with a fluid-filled lumen. The wing pouch tissue is mechanically connected to peripodial tissue via the hinge tissue [52]. The wing disc starts flat and then during development forms folds [52]. The wing pouch starts flat and transforms into a dome [43], raising the question of whether a mechanical instability (elastic buckling) underlies the dome formation [20]. One may speculate that the 3d deformations of the tissue, formed potentially through mechanical instability, may be relevant to size regulation. For instance, the local geometric curvature of the dome

Fit Parameters			Models		
	symbol	unit	Only radial MF	Only MF	MF + basal
			(Figs. 3, 5)	(Fig 6A&B)	(Fig 6C&D)
Homeostatic stress	T^*	kPa	$-2.09 \cdot 10^4$	$-1.00 \cdot 10^2$	$-4.79 \cdot 10^1$
radial growth response	K_R	$kPa^{-1} \text{hours}^{-1}$	$5.01 \cdot 10^{-6}$	$9.51 \cdot 10^{-4}$	$1.73 \cdot 10^{-3}$
tangential growth response	K_θ	$kPa^{-1} \text{hours}^{-1}$	—	$5.23 \cdot 10^{-4}$	$1.45 \cdot 10^{-3}$
rate of basal growth	s	hours^{-1}	—	—	$1.41 \cdot 10^{-3}$

TABLE I. Fit parameters. The model of only radial feedback corresponds to (7) and Figs. 3 and 5. It requires the fitting of two parameters. Similarly, the "Only MF" model corresponds to (5) and (6) and the orange curves in Fig. 6A&B, requiring three fit parameters. Lastly, the robustly size controlled model comprised of mechanical feedback and basal growth corresponds to (10) and the orange curves in Fig. 6C&D, requiring four fit parameters. The data fitted is from [4].

name	symbol	value	reference
Shear modulus	μ	10 kPa	[44, 47, 48]
Initial radius	R_{initial}	2 μm	[40, 49]

TABLE II. Model parameters. The shear modulus for *Drosophila* tissue was calculated in [44, 48] based on measurements of the Young's Modulus via photo-elasticity reported in [47]. To estimate the initial radius of the *Drosophila* wing disc, at which point our mechanical feedback mechanism starts acting, we note that the initial cell assembly is approximately $N = 10$ cells as reported in [49], with a mean apical cell area of approximately $A = 1.25 \mu\text{m}^2$. Assuming that the total initial area of the wing disc is $N \cdot A$, we thus estimate the initial radius as of the wing disc domain as $R_{\text{initial}} = \sqrt{N \cdot A / \pi} = 2 \mu\text{m}$.

may provide an additional length scale that can be exploited in controlling the robustness of a final size, potentially providing an alternative robustness mechanism to the sG term in (10).

It is controversial whether non-uniformity of growth in the *Drosophila* wing disc exists, and is exploited in the buildup of mechanical stress in the wing disc during development. It is widely believed that growth is spatially uniform ([4, 6, 12, 27]), although one report suggests some non-uniformity in early developmental stages ([40]). Older models relying on the assumption of non-uniform growth in the early stages of development, only to be smoothed out by chemo-mechanical feedback in later developmental stages [21, 22] may need to be revisited in light of the now better established spatial uniformity of proliferation rates [4, 27] and the recent quantification of *Dpp* scaling [4]. Instead of transient non-uniformity of growth to explain the buildup of mechanical stress as done in previous models [21, 22], we provide an alternative explanation through growth anisotropy ($\gamma_R \neq \gamma_\theta$) [36] in line with recent experimental observations of the uniformity of proliferation rates.

A major difficulty in directly comparing mechanical models with experimental data is the reconstruction of the mechanical stress tensor. The current standard is to segment the polygonal cell geometry in cross-sections of

the wing pouch and compute pressures in cells and tensions at cell edges. This is an underdetermined inverse problem [2], providing no absolute values of pressures and forces, making it impossible to directly compare force reconstruction data at different developmental times of the same tissue. Furthermore, linking mechanical descriptions at the cell level with the continuum level remains challenging [53, 54]. Novel experimental methods in which forces are measured more directly [55], image reconstruction methods [56], and mathematical methods facilitating the comparison of cell-level to continuum stress [57], as well as 3d vertex models [58] may make it possible to characterise the complex mechanical interaction of peripodial, hinge and pouch tissue in the wing disc. This is a prerequisite to fully understand the nature of buildup of mechanical stress during development and its impact on size regulation.

To address the question if a given mechanical feedback law can robustly encode a final size, Ambrosi et al. [44, 59] formulated a selection criterion. According to their criterion, and in agreement with our results, (1) is not robustly size controlled. Further, they postulated that the gradient of stress, $\text{diag}(\partial_R T_R, \partial_R T_\theta)$, can be used to construct a robustly size controlled growth law. However, no such law has been proposed, and its construction in conjunction with the experimental observation of spatially uniform cell proliferation remains a challenge.

In summary, our analysis demonstrates how a careful choice of mechanical feedback mechanism, consistent with numerous experimental observations about the growth and mechanical stress of the *Drosophila* wing disc, reveals the potential of mechanics as a regulator of the final size of an organ. We anticipate that the continuum framework we propose for modelling morphogenetic dynamics can usefully be extended to other geometrically complex morphogenetic systems, such as the *Drosophila* eye disc [60].

MATERIALS AVAILABILITY

All data needed to evaluate the conclusions in the paper are present in the paper and/or the Supplementary Information. The associated computational codes can be accessed via the github repository <https://github.com/airlich/Drosophila-size-regulation>.

ACKNOWLEDGMENTS

This work was supported by the Momentum Grant by Pierre Recho. I thank Giuseppe Zurlo, Pierre Recho, Stefan Harmansa and Thomas Lecuit for many helpful discussions on size control, both from the theoretical and experimental point of view.

SUPPLEMENTARY INFORMATION

We model the *Drosophila* wing disc as an incompressible isotropic hyperelastic material. The disk growth is modeled through bulk volumetric expansion, which can be spatially inhomogeneous and anisotropic across the growing disk. We restrict to growth and deformations such that the axisymmetric disk geometry is always maintained. Moreover, we assume that there are no external forces, so that any deformation is caused purely by growth and the elastic response. We discuss the details of the model in the following sections. We start in Section S1 ("Geometry") with the kinematics of growth, providing a formal background to the ideas sketched in the main text relating to Fig. 2. Next, in Section S2 ("Mechanics") we derive from a neo-Hookean model the expressions for the deviatoric and hydrostatic parts of the Cauchy stress tensor which were used in Eq. (2)–(4) in the main text. Next, we discuss in Section S3 ("Growth") our *Drosophila* wing disc model in the context of the linear homeostasis growth law, a well-established phenomenological model for growth in biomechanics, which has found great use in modelling morphogenesis and cardiovascular biomechanics. Finally, we conclude in Section S4 ("Size") where we provide explicit solutions of the equations derived in the three preceding sections. This allows us to present the solutions from which the final radius results of the main text, i.e. Eq. (8), (9) and (11) were derived.

S1. GEOMETRY

Geometrically, we work in a planar polar coordinate basis $\{\mathbf{e}_R, \mathbf{e}_\theta\}$ (the same basis vectors apply to both initial and current configurations), in which the deformation can be described by the map \mathbf{x} , mapping vectors from the initial configuration \mathcal{B}_0 to the current configuration \mathcal{B}_t (see Fig. S1). The deformation map $\mathbf{x} : \mathcal{B}_0 \rightarrow \mathcal{B}_t$ given by:

$$\mathbf{x} = r(R, t) \mathbf{e}_R. \quad (\text{S1})$$

For this map, the deformation gradient is

$$\mathbf{F}(R, t) = \frac{\partial r(R, t)}{\partial R} \mathbf{e}_R \otimes \mathbf{e}_R + \frac{r(R, t)}{R} \mathbf{e}_\theta \otimes \mathbf{e}_\theta. \quad (\text{S2})$$

The elastic deformation gradient takes the form

$$\mathbf{A}(R, t) = \alpha_R(R, t) \mathbf{e}_R \otimes \mathbf{e}_R + \alpha_\theta(R, t) \mathbf{e}_\theta \otimes \mathbf{e}_\theta. \quad (\text{S3})$$

Incompressibility requires

$$J_A = \det \mathbf{A}(R, t) = 1, \quad (\text{S4})$$

we thus define $\alpha(R, t) := \alpha_\theta(R, t)$, so that $\alpha^{-1}(R, t) = \alpha_R(R, t)$. We assume a diagonal growth tensor

$$\mathbf{G}(R, t) = \gamma_R(R, t) \mathbf{e}_R \otimes \mathbf{e}_R + \gamma_\theta(R, t) \mathbf{e}_\theta \otimes \mathbf{e}_\theta. \quad (\text{S5})$$

In matrix form (with the basis $\{\mathbf{e}_R, \mathbf{e}_\theta\}$ implied), we have

$$\mathbf{F}(R, t) = \begin{pmatrix} \frac{\partial r(R, t)}{\partial R} & 0 \\ 0 & \frac{r(R, t)}{R} \end{pmatrix}, \quad \mathbf{A}(R, t) = \begin{pmatrix} \alpha^{-1}(R, t) & 0 \\ 0 & \alpha(R, t) \end{pmatrix}, \quad \mathbf{G}(R, t) = \begin{pmatrix} \gamma_R(R, t) & 0 \\ 0 & \gamma_\theta(R, t) \end{pmatrix}. \quad (\text{S6})$$

In the initial (stress-free) reference configuration \mathcal{B}_0 , the domain boundary is located $R = R_{\text{initial}}$. From the morphoeastic decomposition $\mathbf{F} = \mathbf{AG}$, we find $\frac{\partial r(R, t)}{\partial R} = \gamma_R(R, t) / \alpha(R, t)$ and $r(R, t) / R = \alpha(R, t) \gamma_\theta(R, t)$. By eliminating $\alpha(R, t)$, we obtain

$$r(R, t) \frac{\partial r(R, t)}{\partial R} = \frac{\gamma_R(R, t) \gamma_\theta(R, t)}{R}, \quad r(R = 0, t) = 0. \quad (\text{S7})$$

Here we prescribed at the disk center ($R = 0$) a no-displacement boundary condition $r(R = 0, t) = 0$ for all t .

S2. MECHANICS

In this section we state a boundary value problem for stress and displacement, and its explicit solution for the case that the growth tensor \mathbf{G} is spatially uniform. More general cases with multiple domains have been reported in

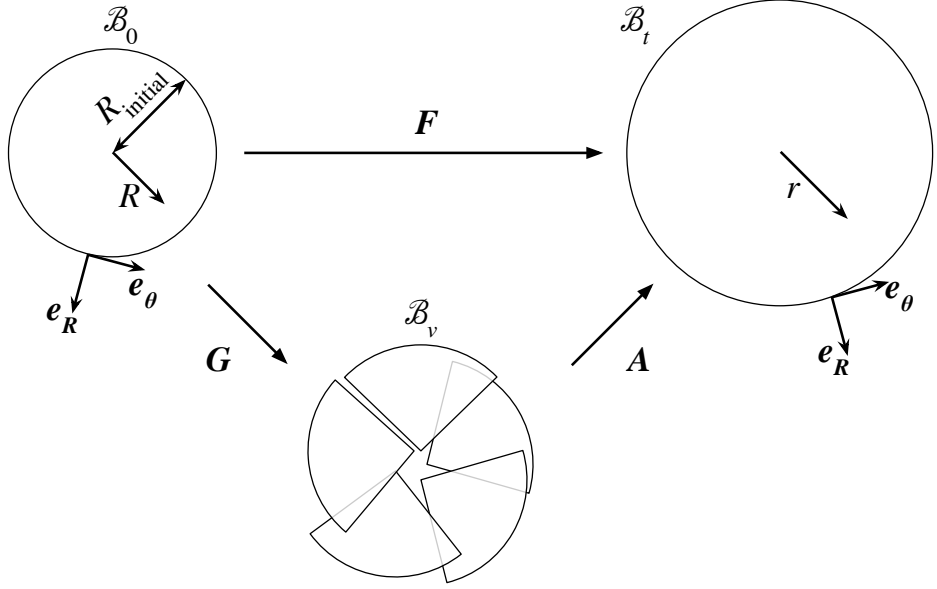


FIG. S1. Sketch of morphoelastic decomposition. In the initial configuration \mathcal{B}_0 the disk is unstressed and undeformed, corresponding to the pre-growth stage. The disk has radius R_{initial} and the position along the disk is denoted R , which is in the range $0 \leq R \leq R_{\text{initial}}$. The growth tensor \mathbf{G} instructs how vectors from \mathcal{B}_0 are mapped into the virtual configuration, \mathcal{B}_v , and the elastic deformation gradient \mathbf{A} maps vectors from \mathcal{B}_v to the current configuration, \mathcal{B}_t . In the current configuration, the disk at time t has the radius $r(R_{\text{initial}}, t)$.

[36, 44], we derive here the relevant subcase for our model. Given that all deformations are diagonal in the coordinate basis considered here, the Cauchy stress is also diagonal

$$\mathbf{T}(R, t) = T_R(R, t) \mathbf{e}_R \otimes \mathbf{e}_R + T_\theta(R, t) \mathbf{e}_\theta \otimes \mathbf{e}_\theta. \quad (\text{S8})$$

Let $W(\alpha_R(R, t), \alpha_\theta(R, t))$ be the strain-energy density, which relates to the Cauchy stress tensor by $\mathbf{T}(R, t) = \mathbf{A}(R, t) W_{\mathbf{A}}(R, t) - p(R, t) \mathbf{1}$, where $p(R, t)$ is the Lagrange multiplier enforcing incompressibility. In components, this reads

$$T_R(R, t) = \alpha_R(R, t) \frac{\partial W}{\partial \alpha_R}(R, t) - p(R, t), \quad T_\theta(R, t) = \alpha_\theta(R, t) \frac{\partial W}{\partial \alpha_\theta}(R, t) - p(R, t). \quad (\text{S9})$$

With no external loads, mechanical equilibrium requires $\text{div } \mathbf{T}(R, t) = 0$, which takes the form

$$\frac{\partial T_R(R, t)}{\partial r(R, t)} = \frac{T_\theta(R, t) - T_R(R, t)}{r(R, t)}. \quad (\text{S10})$$

Defining $\widehat{W}(\alpha(R, t)) := W(\alpha^{-1}(R, t), \alpha(R, t))$, we have

$$T_\theta(R, t) - T_R(R, t) = \alpha(R, t) \widehat{W}'(\alpha(R, t)). \quad (\text{S11})$$

The above formulation is valid for all isotropic, incompressible material. We further restrict it to the simplest possible material model of a neo-Hookean quadratic strain-energy density given by:

$$W = \frac{\mu}{2} (\alpha_R^2(R, t) + \alpha_\theta^2(R, t) - 2), \quad (\text{S12})$$

where μ is the shear modulus of the material. In this case,

$$\widehat{W}(\alpha(R, t)) = \frac{\mu}{2} (\alpha^2(R, t) + \alpha^{-2}(R, t) - 2), \quad (\text{S13})$$

for which (S10) becomes

$$\frac{\partial T_R(R, t)}{\partial R} = \frac{\mu \gamma_R(R, t)}{R \gamma_\theta(R, t)} \left(1 - \frac{R^4 \gamma_\theta^4(R, t)}{r^4(R, t)} \right), \quad T_R(R_{\text{initial}}, t) = 0. \quad (\text{S14})$$

Here we imposed that the boundary of the disk is stress-free for all times, that is $T_R(R_{\text{initial}}, t) = 0$. Equations (S7) and (S14) completely determine the deformation and stress state. Due to the fixed inner boundary condition, for a given growth tensor (S7) can be integrated separately, i.e. the deformation is determined independently from the stress, and the radial Cauchy stress is then determined by integrating (S14). Once the radial stress component T_R is determined, the circumferential component satisfies

$$T_\theta(R, t) = T_R(R, t) + \frac{\mu r^2(R, t)}{R^2 \gamma_\theta^2(R, t)} \left(1 - \frac{R^4 \gamma_\theta^4(R, t)}{r^4(R, t)} \right). \quad (\text{S15})$$

Note also that for constant γ_R and γ_θ , these integrals may be performed analytically, giving explicit expressions for the stress and deformation in terms of the growth.

Consistent with the observation that growth rates over the *Drosophila* wing disc are spatially uniform [12, 24, 25], we assume that the growth rates γ_R and γ_θ are independent of R . Then the boundary value problem (S7), (S14) has the solution

$$r(R) = R \sqrt{\gamma_R \gamma_\theta} \quad (\text{S16})$$

$$T_{RR}(R) = \mu \left(\frac{\gamma_R}{\gamma_\theta} - \frac{\gamma_\theta}{\gamma_R} \right) \log \left(\frac{R}{R_{\text{initial}}} \right) \quad (\text{S17})$$

$$T_{\theta\theta}(R) = \mu \left(\frac{\gamma_R}{\gamma_\theta} - \frac{\gamma_\theta}{\gamma_R} \right) \left(\log \left(\frac{R}{R_{\text{initial}}} \right) + 1 \right) \quad (\text{S18})$$

When the stress tensor is decomposed into deviatoric and hydrostatic part $\mathbf{T} = \mathbf{T}_{\text{dev}} + \mathbf{T}_{\text{hyd}}$, the results from the main text (2), (3) and (4) are retrieved.

S3. GROWTH

The linear homeostasis growth law, a term coined in [28], is a phenomenological hypothesis inspired by the observation that tissue stretching stimulates cell proliferation, whereas compression inhibits it. The growth law reads

$$\dot{\mathbf{G}} \mathbf{G}^{-1} = \mathcal{K} : (\mathbf{M} - \mathbf{M}^*). \quad (\text{S19})$$

Here \mathbf{G} is the growth deformation [16], \mathcal{K} is a fourth-order coefficient tensor, \mathbf{M} is the Mandel stress tensor, and \mathbf{M}^* the homeostatic value of the Mandel stress. This growth law, or variations of it, have been applied to modelling many problems in biomechanics. It has been applied to different morphogenesis problems, like sea urchin gastrulation [31], the formation of ribs in Ammonite's seashells [45], and the intestinal crypt [46]. Further applications involve tumors [37, 61] and the cardiovascular system [15, 18, 19, 62–64], as well as wound healing [31, 35], and discrete networks such as plant cell networks [54]. Variations of the growth law (S19) have been proposed as natural descriptors of growth based on thermodynamics arguments [33, 65, 66]. We next describe how the growth law (1) based on deviatoric stress proposed in the main text can be retrieved from the homeostatic growth law (S19). Further, we elaborate how the choice of its coefficients \mathbf{K} in (1) leads to the growth law (5) and (6) discussed in detail in the main text.

First, we note that the Mandel stress is defined as

$$\mathbf{M} = J_A^{-1} \mathbf{A}^T \mathbf{T} \mathbf{A}^{-T}, \quad (\text{S20})$$

In the present setting, the tensors \mathbf{A} (see (S3)) and \mathbf{T} (see (S8)) are diagonal in the polar coordinate basis, thus they are coaxial and commute, $\mathbf{A}\mathbf{T} = \mathbf{T}\mathbf{A}$. Furthermore, we are considering an incompressible material (S4). As a results, in our setting Cauchy and Mandel stress are identical, $\mathbf{A} = \mathbf{T}$.

Further, we choose the following non-vanishing components of the fourth order tensor \mathcal{K} , which are assumed to be constants in space and time:

$$K_{RR} = \mathcal{K}_{RRRR}, \quad K_{R\theta} = \mathcal{K}_{RR\theta\theta}, \quad K_{\theta R} = \mathcal{K}_{\theta\theta RR}, \quad K_{\theta\theta} = \mathcal{K}_{\theta\theta\theta\theta}. \quad (\text{S21})$$

Then the growth law (S19) reads

$$\dot{\gamma}_R \gamma_R^{-1} = K_{RR} (T_R - T_R^*) + K_{R\theta} (T_\theta - T_\theta^*) \quad (\text{S22})$$

$$\dot{\gamma}_\theta \gamma_\theta^{-1} = K_{\theta R} (T_R - T_R^*) + K_{\theta\theta} (T_\theta - T_\theta^*) \quad (\text{S23})$$

We note that the hydrostatic stress is $\mathbf{T}_{\text{hyd}} = \frac{1}{2}(\text{tr } \mathbf{T}) \mathbf{1}$ (where the identity is $\mathbf{1} = \delta_{ij} \mathbf{e}_i \otimes \mathbf{e}_j$) and the deviatoric stress is $\mathbf{T}_{\text{dev}} = \mathbf{T} - \frac{1}{2}(\text{tr } \mathbf{T}) \mathbf{1}$. Explicitly:

$$\mathbf{T}_{\text{dev}} = \begin{pmatrix} \frac{T_R - T_\theta}{2} & 0 \\ 0 & -\frac{T_R - T_\theta}{2} \end{pmatrix}, \quad \mathbf{T}_{\text{hyd}} = \begin{pmatrix} \frac{T_R + T_\theta}{2} & 0 \\ 0 & \frac{T_R + T_\theta}{2} \end{pmatrix}. \quad (\text{S24})$$

It follows that to arrive at the deviatoric stress-driven growth law (1), we must have $K_{R\theta} = -K_{RR}$ and $K_{\theta R} = -K_{\theta\theta}$. We further define the maximal shear stress T_{max} as well as the homeostatic stress T^*

$$T_{\text{max}} = \frac{T_R - T_\theta}{2}, \quad T^* = \frac{T_R^* - T_\theta^*}{2}. \quad (\text{S25})$$

Now, to derive from (S22) and (S23) a growth law depending on deviatoric stress, we choose the coefficients

$$K_{RR} = K_R/2, \quad K_{\theta\theta} = -K_\theta/2, \quad (\text{S26})$$

leading to the growth law (5), (6) discussed in detail in the main text.

S4. SIZE

The model (7) can be solved analytically for $\gamma_R(t)$. Using Eq. (S16) with the assumption that the initial radius is R_{initial} , we obtain the evolving domain radius

$$r(R_{\text{initial}}, t) = \frac{R_{\text{initial}}}{\sqrt{2\mu}} \sqrt{\sqrt{4\mu^2 + (T^*)^2} \tanh \left[\frac{1}{2} K_R t \sqrt{4\mu^2 + (T^*)^2} + \tanh^{-1} \left(\frac{2\mu + T^*}{\sqrt{4\mu^2 + (T^*)^2}} \right) \right] - T^*} \quad (\text{S27})$$

which is a function of time t , radial growth rate K_R , the homeostatic stress T^* , and the shear modulus of the tissue μ . This functional form underlies the sigmoid-type curve shown in Fig. 3. By taking the limit $t \rightarrow \infty$ of this expression we can find the asymptotic domain radius, i.e. the disc radius at growth termination, given as R_{final} in Eq. (8).

By computing the extremum of (S27), which requires solving $\ddot{r}(t_{\text{inflection}}) = 0$ for $t_{\text{inflection}}$, we can obtain the full form of the function f given in (9), which is

$$f(T^*, \mu) = -\frac{2 \text{ArcTanh} \left(\frac{2\mu + T^*}{\sqrt{4\mu^2 + (T^*)^2}} \right)}{K_R \sqrt{4\mu^2 + (T^*)^2}}. \quad (\text{S28})$$

We also note that an analysis of the equilibrium state of (5) and (6), that is $\dot{\gamma}_R = \dot{\gamma}_\theta = 0$, yields

$$\frac{\gamma_\theta}{\gamma_R} = \frac{\sqrt{4\mu^2 + (T^*)^2} + T^*}{2\mu} \quad (\text{S29})$$

which is the slope of the dashed line in Fig. 6B.

Finally, we consider an equilibrium analysis ($\dot{\gamma}_R = \dot{\gamma}_\theta = 0$) of the same model amended with the basal growth term:

$$\dot{\gamma}_R \gamma_R^{-1} = K_R (T_{\text{max}} - T^*) - s \gamma_R \quad (\text{S30})$$

$$\dot{\gamma}_\theta \gamma_\theta^{-1} = K_\theta (T_{\text{max}} - T^*) - s \gamma_\theta. \quad (\text{S31})$$

The only equilibrium is at

$$\gamma_R = \frac{K_\theta^2 \mu - \mu K_R^2 - K_\theta K_R T^*}{K_\theta s}, \quad \gamma_\theta = \frac{K_\theta^2 \mu - \mu K_R^2 - K_\theta K_R T^*}{K_R s}. \quad (\text{S32})$$

Taking into account the solution $r = R \sqrt{\gamma_R \gamma_\theta}$ according to (S16), we recover the final wing disc size for the model with mechanical feedback and basal growth, given in the main text Eq. (11).

[1] U. Nienhaus, T. Aegerter-Wilmsen, and C. M. Aegerter, Mechanisms of development **126**, 942 (2009).

[2] S. Ishihara and K. Sugimura, *Journal of theoretical biology* **313**, 201 (2012).

[3] J. Travis, “Mysteries of development,” (2013).

[4] O. Wartlick, P. Mumcu, A. Kicheva, T. Bittig, C. Seum, F. Jülicher, and M. Gonzalez-Gaitan, *Science* **331**, 1154 (2011).

[5] T. Aegerter-Wilmsen, M. B. Heimlicher, A. C. Smith, P. B. de Reuille, R. S. Smith, C. M. Aegerter, and K. Basler, *Development* **139**, 3221 (2012).

[6] J. Vollmer, F. Casares, and D. Iber, *Open biology* **7**, 170190 (2017).

[7] S. J. Day and P. A. Lawrence, *Development* **127**, 2977 (2000).

[8] S. Restrepo, J. J. Zartman, and K. Basler, *Current Biology* **24**, R245 (2014).

[9] L. LeGoff and T. Lecuit, *Cold Spring Harbor perspectives in biology* **8**, a019232 (2016).

[10] N. Hervieux, M. Dumond, A. Sapala, A.-L. Routier-Kierzkowska, D. Kierzkowski, A. H. Roeder, R. S. Smith, A. Boudaoud, and O. Hamant, *Current Biology* **26**, 1019 (2016).

[11] G. Helmlinger, P. A. Netti, H. C. Lichtenbeld, R. J. Melder, and R. K. Jain, *Nature biotechnology* **15**, 778 (1997).

[12] D. Eder, C. Aegerter, and K. Basler, *Mechanisms of development* **144**, 53 (2017).

[13] Y.-C. Fung, in *Theoretical, Experimental, and Numerical Contributions to the Mechanics of Fluids and Solids* (Springer, 1995) pp. 469–482.

[14] F.-H. Hsu, *Journal of biomechanics* **1**, 303 (1968).

[15] A. Rachev, *Journal of biomechanics* **30**, 819 (1997).

[16] E. K. Rodriguez, A. Hoger, and A. D. McCulloch, *Journal of biomechanics* **27**, 455 (1994).

[17] L. A. Taber, *Journal of theoretical biology* **193**, 201 (1998).

[18] L. A. Taber, *Applied Mechanics Reviews* **48**, 487 (1995).

[19] L. A. Taber and D. W. Eggers, *Journal of theoretical biology* **180**, 343 (1996).

[20] B. I. Shraiman, *Proceedings of the National Academy of Sciences of the United States of America* **102**, 3318 (2005).

[21] L. Hufnagel, A. A. Teleman, H. Rouault, S. M. Cohen, and B. I. Shraiman, *Proceedings of the National Academy of Sciences* **104**, 3835 (2007).

[22] T. Aegerter-Wilmsen, C. M. Aegerter, E. Hafen, and K. Basler, *Mechanisms of development* **124**, 318 (2007).

[23] S. Dupont, L. Morsut, M. Aragona, E. Enzo, S. Giulitti, M. Cordenonsi, F. Zanconato, J. Le Digabel, M. Forcato, S. Bicciato, *et al.*, *Nature* **474**, 179 (2011).

[24] K. D. Irvine and B. I. Shraiman, *Development* **144**, 4238 (2017).

[25] J. Gou, J. A. Stotsky, and H. G. Othmer, *Wiley Interdisciplinary Reviews: Systems Biology and Medicine* **12**, e1478 (2020).

[26] D. Aguilar-Hidalgo, S. Werner, O. Wartlick, M. González-Gaitán, B. M. Friedrich, and F. Jülicher, *Physical review letters* **120**, 198102 (2018).

[27] G. Schwank, G. Tauriello, R. Yagi, E. Kranz, P. Koumoutsakos, and K. Basler, *Developmental cell* **20**, 123 (2011).

[28] A. Goriely, *The mathematics and mechanics of biological growth*, Vol. 45 (Springer, 2017).

[29] D. Ambrosi, M. Ben Amar, C. J. Cyron, A. DeSimone, A. Goriely, J. D. Humphrey, and E. Kuhl, *Journal of the Royal Society Interface* **16**, 20190233 (2019).

[30] L. A. Taber, *Biomechanics and modeling in mechanobiology* **7**, 427 (2008).

[31] L. A. Taber, *Philosophical Transactions of the Royal Society A: Mathematical, Physical and Engineering Sciences* **367**, 3555 (2009).

[32] A. Ramasubramanian and L. a. Taber, *Biomechanics and modeling in mechanobiology* **7**, 77 (2008).

[33] D. Ambrosi and F. Guana, *Mathematics and Mechanics of Solids* **12**, 319 (2005).

[34] R. Vandiver and A. Goriely, *J. Biol. Dyn.* **3**, 180 (2009).

[35] L. G. Bowden, H. M. Byrne, P. K. Maini, and D. E. Moulton, *Biomechanics and modeling in mechanobiology* , 1 (2015).

[36] A. Erlich, D. E. Moulton, and A. Goriely, *Bulletin of mathematical biology* **81**, 3219 (2019).

[37] M. Basan, T. Risler, J.-F. Joanny, X. Sastre-Garau, and J. Prost, *HFSP journal* **3**, 265 (2009).

[38] M. Epstein and G. a. Maugin, *International Journal of Plasticity* **16**, 951 (2000).

[39] N. A. Dye, M. Popovic, K. V. Iyer, S. Eaton, and F. Julicher, *BioRxiv* (2020).

[40] Y. Mao, A. L. Tournier, A. Hoppe, L. Kester, B. J. Thompson, and N. Tapon, *The EMBO journal* **32**, 2790 (2013).

[41] A. Nestor-Bergmann, G. A. Stooke-Vaughan, G. K. Goddard, T. Starborg, O. E. Jensen, and S. Woolner, *Cell reports* **26**, 2088 (2019).

[42] A. Nestor-Bergmann, G. Goddard, S. Woolner, and O. E. Jensen, *Mathematical medicine and biology: a journal of the IMA* **35**, 11 (2018).

[43] L. LeGoff, H. Rouault, and T. Lecuit, *Development* **140**, 4051 (2013).

[44] D. Ambrosi, V. Pettinati, and P. Ciarletta, *International Journal of Non-Linear Mechanics* **75**, 5 (2015).

[45] A. Erlich, R. Howell, A. Goriely, R. Chirat, and D. E. Moulton, *The ANZIAM Journal* **59**, 581 (2018).

[46] A. A. Almet, H. M. Byrne, P. K. Maini, and D. E. Moulton, *arXiv preprint arXiv:2006.00172* (2020).

[47] T. Schluck and C. Aegerter, *The European Physical Journal E* **33**, 111 (2010).

[48] V. Pettinati, D. Ambrosi, P. Ciarletta, and S. Pezzuto, *Computer methods in biomechanics and biomedical engineering* **19**, 1241 (2016).

[49] M. Milán, S. Campuzano, and A. García-Bellido, *Proceedings of the National Academy of Sciences* **93**, 640 (1996).

[50] I. Averbukh, D. Ben-Zvi, S. Mishra, and N. Barkai, *Development* **141**, 2150 (2014).

[51] A. Fruleux and A. Boudaoud, *Proceedings of the National Academy of Sciences* **116**, 1940 (2019).

[52] M. Tozluoğlu, M. Duda, N. J. Kirkland, R. Barrientos, J. J. Burden, J. J. Muñoz, and Y. Mao, *Developmental cell* **51**, 299 (2019).

- [53] N. Murisic, V. Hakim, I. G. Kevrekidis, S. Y. Shvartsman, and B. Audoly, *Biophysical journal* **109**, 154 (2015).
- [54] A. Erlich, G. W. Jones, F. Tisseur, D. E. Moulton, and A. Goriely, *Proceedings of the Royal Society A* **476**, 20190523 (2020).
- [55] K. Bambadekar, R. Clément, O. Blanc, C. Chardès, and P.-F. Lenne, *Proceedings of the National Academy of Sciences* **112**, 1416 (2015).
- [56] N. Noll, S. J. Streichan, and B. I. Shraiman, *Physical Review X* **10**, 011072 (2020).
- [57] O. E. Jensen, E. Johns, and S. Woolner, *Proceedings of the Royal Society A* **476**, 20190716 (2020).
- [58] P. Gómez-Gálvez, P. Vicente-Munuera, A. Tagua, C. Forja, A. M. Castro, M. Letrán, A. Valencia-Expósito, C. Grima, M. Bermúdez-Gallardo, Ó. Serrano-Pérez-Higueras, *et al.*, *Nature communications* **9**, 1 (2018).
- [59] D. Ambrosi, L. Belousov, and P. Ciarletta, *Meccanica* **52**, 3371 (2017).
- [60] P. Fried, M. Sánchez-Aragón, D. Aguilar-Hidalgo, B. Lehtinen, F. Casares, and D. Iber, *PLoS computational biology* **12**, e1005052 (2016).
- [61] D. Ambrosi and F. Mollica, *Journal of mathematical biology* **48**, 477 (2004).
- [62] P. W. Alford, J. D. Humphrey, and L. A. Taber, *Biomechanics and modeling in mechanobiology* **7**, 245 (2008).
- [63] S. Göktepe, O. J. Abilez, K. K. Parker, and E. Kuhl, *Journal of theoretical biology* **265**, 433 (2010).
- [64] L. Taber and S. Chabert, *Biomechanics and modeling in mechanobiology* **1**, 29 (2002).
- [65] D. Ambrosi and A. Guillou, *Continuum Mechanics and Thermodynamics* **19**, 245 (2007).
- [66] D. Ambrosi, A. Guillou, and E. Di Martino, *Biomechanics and modeling in mechanobiology* **7**, 63 (2008).